MCB
Journals.ASM.org

The Conserved Bud20 Zinc Finger Protein Is a New Component of the Ribosomal 60S Subunit Export Machinery

Jochen Baßler,[a] Isabella Klein,[b] Claudia Schmidt,[b] Martina Kallas,[a] Emma Thomson,[a] Maria Anna Wagner,[b] Bettina Bradatsch,[a] Gerald Rechberger,[b] Heimo Strohmaier,[c] Ed Hurt,[a] and Helmut Bergler[b]

Biochemie-Zentrum der Universität Heidelberg, Heidelberg, Germany[a]; Institut für Molekulare Biowissenschaften, Karl-Franzens Universität Graz, Graz, Austria[b]; and Zentrum für Medizinische Grundlagenforschung, Medizinische Universität Graz, Graz, Austria[c]

The nuclear export of the preribosomal 60S (pre-60S) subunit is coordinated with late steps in ribosome assembly. Here, we show that Bud20, a conserved C_2H_2-type zinc finger protein, is an unrecognized shuttling factor required for the efficient export of pre-60S subunits. Bud20 associates with late pre-60S particles in the nucleoplasm and accompanies them into the cytoplasm, where it is released through the action of the Drg1 AAA-ATPase. Cytoplasmic Bud20 is then reimported via a Kap123-dependent pathway. The deletion of Bud20 induces a strong pre-60S export defect and causes synthetic lethality when combined with mutant alleles of known pre-60S subunit export factors. The function of Bud20 in ribosome export depends on a short conserved N-terminal sequence, as we observed that mutations or the deletion of this motif impaired 60S subunit export and generated the genetic link to other pre-60S export factors. We suggest that the shuttling Bud20 is recruited to the nascent 60S subunit via its central zinc finger rRNA binding domain to facilitate the subsequent nuclear export of the preribosome employing its N-terminal extension.

The ribosome is the cellular machine responsible for the correct translation of genetic information into the amino acid sequences of proteins. The 80S ribosome of eukaryotes is composed of one 40S subunit and one 60S subunit, which contain four different rRNA species and about 80 ribosomal proteins (r-proteins). The correct assembly of r-proteins and rRNA into ribosomal subunits is a highly dynamic process that requires the coordinated action of a large number of *trans*-acting factors, the vast majority of which are essential for the survival of the organism (for recent reviews on ribosome biogenesis, see references 8, 10, 19, 27, 29, and 52). Moreover, it has become evident that ribosome biogenesis is tightly regulated in order to supply actively dividing cells with sufficient levels of ribosomal subunits. Accordingly, one characteristic feature of cancer cells is an elevated level of ribosome biogenesis factors. In the converse situation, defects in ribosome assembly result in several hereditary human diseases, collectively called ribosomopathies (reviewed in references 9 and 38). Thus, a molecular comprehension of ribosome biogenesis will stimulate the development of novel therapies for cancer and ribosomopathies. Most of our knowledge on ribosome biogenesis is based on studies in *Saccharomyces cerevisiae.* In this organism, about 2,000 ribosomes are synthesized every minute, which makes ribosome biogenesis a major energy-consuming process in the cell (55).

During the course of maturation, the emerging ribosomal subunits transit from the nucleolus via the nucleoplasm into the cytoplasm. On this path, *trans*-acting factors join the preribosomal particles to mediate rRNA processing, the modification and restructuring of rRNA precursors, and their assembly with ribosomal proteins, before they dissociate again to enter a new cycle of ribosome biogenesis. At least for some protein factors, this dissociation requires an input of energy, which is provided by ATP-hydrolyzing enzymes, like the AAA-ATPases Rix7, Rea1, and Drg1, which are essential for the removal of tightly associated protein factors to ensure the progression of ribosome formation (3, 28, 30, 42, 54).

While most of these *trans*-acting factors leave preribosomal particles within the nucleus, a few of them accompany the ribosomal subunits through the nuclear pores into the cytoplasm. Some factors participate in ribosome export through the nuclear pore complex (NPC), whereas others engage in cytoplasmic ribosome maturation events (41).

The NPC in yeast is a 66-MDa macromolecular structure that exhibits octagonal symmetry and is built up from multiples of about 30 different proteins. It spans the nuclear membrane to allow exchange between the nucleoplasm and cytoplasm. The transport channel is lined with phenylalanine-glycine repeat-containing proteins (FG-repeat nucleoporins) that form a hydrophobic meshwork preventing the free diffusion of large proteins (57). The export of large proteins and protein complexes is mediated by specific export factors, which interact with these FG repeats. The export of preribosomal 60S (pre-60S) particles requires the exportin Xpo1/Crm1, which binds to the adaptor protein Nmd3 to mediate RanGTP-dependent export (11, 21). Furthermore, the Mex67-Mtr2 heterodimer, originally implicated in mRNA export, and the nonessential protein Arx1 also interact with FG-repeat Nups and act as additional export factors for the pre-60S particle in a RanGTP-independent manner (1, 6, 24, 59). In addition, Ecm1 is required for efficient pre-60S subunit export (60). Thus, due to its huge size, the pre-60S particle apparently requires several transport receptors for efficient export toward the cytoplasm (6, 44).

Received 6 July 2012 Returned for modification 30 July 2012
Accepted 17 September 2012
Published ahead of print 8 October 2012
Address correspondence to Jochen Baßler, jochen.bassler@bzh.uni-heidelberg.de, or Helmut Bergler, helmut.bergler@uni-graz.at.

doi:10.1128/MCB.00910-12

Maturation factors accompanying the pre-60S particle into the cytoplasm, but with no direct implication in export, include Nog1, Rlp24, Tif6, Alb1, and Mrt4. These shuttling proteins are released in late pre-60S maturation steps in the cytoplasm and recycled into the nucleus, where they join pre-60S particles for a new round of ribosome biogenesis. The release of shuttling proteins is achieved by cytoplasmic maturation factors and seems to be required for the incorporation of the last ribosomal proteins into nascent pre-60S particles (18, 26, 33, 42). A key player in cytoplasmic pre-60S maturation is the AAA-ATPase Drg1. This protein binds to the pre-60S particle shortly after export and is required for the release of shuttling proteins and the transition of the particle to more mature forms (32, 42).

Work from different laboratories over the past years underlined the importance of cytoplasmic maturation steps for the formation of functional 60S subunits (reviewed in reference 41). Astonishingly, it remains unclear how many maturation factors actually accompany the pre-60S particle into the cytoplasm and which of them are required for efficient export. This is due mainly to the short residence time of most of these factors in the cytoplasm before reimport into the nucleus, which complicates their detection in the cytoplasm. Here, we report on Bud20 and its role in pre-60S subunit maturation in the yeast *S. cerevisiae*. The use of the recently described anchor-away technology (16) allowed us to demonstrate that Bud20 belongs to the group of shuttling pre-60S biogenesis factors. Bud20 accompanies the pre-60S particle into the cytoplasm and is released shortly after export. Bud20 exhibits a strong genetic interaction with known export factors and is required for the nuclear export of the pre-60S subunit. This function of Bud20 in pre-60S export depends on a conserved sequence stretch in the N-terminal region of the protein, which is partially related to nuclear export signal (NES) sequences.

MATERIALS AND METHODS

Strain construction. Strains used in this study are listed in Table 1. Plasmids used in this study are described in Table 2. Double-deletion strains were generated as described previously (51). Chromosomal deletion mutants were generated by using homologous recombination with linear PCR-amplified DNA fragments as substrates for transformation (34). Correct deletions were verified by PCR or by Western blot analysis. FRB (FKBP12-rapamycin binding domain)-green fluorescent protein (GFP) fusion strains were constructed by the linear transformation of strain HHY110 with PCR products obtained with gene-specific primers and plasmid pFA6-FRG-GFP (16) as the template. The selection of transformants was performed on yeast extract-peptone-dextrose (YPD) plates containing 300 mg/liter Geneticin G415 after a 16-h regeneration period on YPD plates in the absence of selective pressure. Transformants were confirmed by visual inspection for GFP fluorescence and colony PCR with gene-specific forward primers, targeting sequences approximately 300 nucleotides (nt) upstream of the integration site, and a reverse primer hybridizing within the GFP sequence (16). Transformants were tested for growth behavior on YPD plates at 25°C, 30°C, or 37°C and on plates containing rapamycin.

Yellow fluorescent protein (YFP) strains were generated in *drg1-18* mutant strain FWY111 and the isogenic W303 strains (61), as described above, with the exception that plasmid pDH5 (NCRR Yeast Resource Center, University of Washington [http://depts.washington.edu/yeastrc/]) was used as a PCR template. This plasmid contains a pH-tolerant YFP gene for chromosomal tagging and the *Schizosaccharomyces pombe HIS5* gene as a selection marker that complements *S. cerevisiae his3* mutants.

Microscopy and rapamycin treatment. Anchor strains were grown at 30°C overnight in the synthetic dextrose medium SDC, containing 3-fold the amount of adenine to suppress the formation of the vacuolar pigment characteristic of *ade2* strains. After dilution into fresh media and incubation at 30°C, early-log-phase cultures (optical density at 600 nm [OD_{600}] of about 0.4) were treated with 1 μg/ml rapamycin for up to 2 h and inspected for GFP fluorescence. Microscopy was performed by using a 63× Plan-Neofluar objective (Zeiss) mounted on a Zeiss Axioskop fluorescence microscope, a 10× projective, 1.6-fold secondary enlargement lens, and a narrow-band enhanced GFP (eGFP) or YFP filter set (Zeiss). Pictures were exposed by using a cooled charge-coupled-device (CCD) camera (Spot) with an exposure time of 3,500 ms.

In the case of *drg1-18* mutants, strains were grown in SDC medium to the early log phase at 25°C. Cultures were then shifted to the restrictive temperature in a shaking water bath at 37°C for 1 h before aliquots of the cultures were inspected by fluorescence microscopy. To monitor preribosome export defects, strains were transformed with centromeric plasmids expressing the Rpl25-GFP or Rps2-GFP reporter under the control of the native promoter. Cells were grown at 30°C in synthetic dextrose medium lacking Ura (SDC−Ura) to the early logarithmic phase. Fluorescence microscopy was performed by using a narrow-band YFP or eGFP filter set (Zeiss).

TAP purification of preribosomal particles. Affinity purifications of pre-60S particles from YFP-tagged Bud20 *drg1-18* and *DRG1* strains expressing Arx1-tandem affinity purification protein (TAP) started from 1 liter of early-log-phase cultures in YPD after a 1-h shift to 37°C in a shaking water bath. Cells were harvested by centrifugation at 4,000 × *g* for 5 min in 1-liter polycarbonate beakers in a Beckmann centrifuge at 25°C. Cell pellets were washed in cold buffer A and frozen immediately at −70°C. TAP purification of early and late pre-60S particles from TAP-tagged strains started from 2 to 4 liters of log-phase (OD_{600} of about 1.5) cultures grown in YPD at 25°C. Tandem affinity purification was performed as described previously (42).

Liquid chromatography (LC)-MS/MS analysis. Protein spots were excised from gels and tryptically digested according to a method described previously (50). Peptide extracts were dissolved in 0.1% formic acid, separated on a nano-high-performance liquid chromatography (nano-HPLC) system (Ultimate 3000; LC Packings, Amsterdam, Netherlands), and analyzed with a Thermo-Finnigan LTQ linear ion trap mass spectrometer (Thermo, San Jose, CA). The tandem mass spectrometry (MS/MS) data were analyzed by searching the NCBI nonredundant public database with SpectrumMill Rev. 03.03.078 (Agilent, Darmstadt, Germany) software (5). Acceptance parameters were 3 or more identified distinct peptides, according methods described previously (7).

Sucrose gradient analysis. Cells for sucrose gradient analysis were grown in YPD to an OD of 0.6 to 0.8 and treated with cycloheximide for 15 min. Cells were lysed with glass beads by vortexing four times for 30 s. The supernatants were applied onto 10 to 50% sucrose gradients and spun for 16 h at 27,000 rpm in a Beckman SW40 rotor. Profile recording and fractionation were done by using a Foxy Junior instrument from ISCO (for a detailed protocol, see reference 1).

RESULTS

Bud20 is a novel 60S biogenesis factor. Bud20 is a predominantly nuclear protein (23, 39) (Fig. 1A) that was initially described to play a role in bud site selection in *S. cerevisiae* (39). Our laboratory identified *BUD20* in a synthetic lethal (SL) screen with a mutant allele of the Nug1 GTPase (2), suggesting that the protein plays a role in ribosome biogenesis. Bud20 contains a classical C_2H_2 zinc finger and is highly conserved among eukaryotes (Fig. 1B). The nuclear magnetic resonance (NMR) structure of the putative human ortholog ZNF593 revealed a classical zinc finger structure flanked by disordered N- and C-terminal tails of about 40 amino acids (17). Figure 1C

TABLE 1 Yeast strains used in this study

Strain	Genotype	Reference or source
Y3307 Mex67 shuffle bud20Δ	*MAT***a** *mex67*::*HIS3 bud20*::*KanMX his3 trp1 leu2 ura3* pRS316-MEX67	This study
Y3308 Mtr2 shuffle bud20Δ	*MAT*α *mtr2*::*HIS3 bud20*::*KanMX his3 trp1 leu2 ura3* pRS316-MTR2	This study
Y3306 Nmd3 shuffle bud20Δ	*MAT***a** *nmd3*::*KanMX bud20*::*KanMX his3 trp1 leu2 ura3* pRS316-NMD3	This study
Y3310 Ecm1 shuffle bud20Δ	*MAT***a** *ecm1*::*KanMX bud20*::*KanMX his3 trp1 leu2 ura3* pURA3-ADE3-ECM1	This study
Y3294 arx1Δ bud20Δ	*MAT***a** *bud20*::*KanMX arx1*::*KanMX his3 trp1 leu2 ura3*	This study
Y3033 Noc3 shuffle bud20Δ	*bud20*::*KanMX noc3*::*HIS3 trp1 leu2 ade2 ura3* pRS316 *NOC3*	This study
Y2929 Dbp10 shuffle bud20Δ	*MAT***a** *dbp10*::*KanMX bud20*::*KanMX his3 trp1 leu2 ura3* pRS316 *DBP10*	This study
Y2787 Bud20 TAP	*MAT*α *bud20*::*KanMX his3 trp1 leu2 ura3* pRS315 BUD20-TAP	This study
Y5130 Ssf1-TAP Bud20-HA	*MAT*α *Ssf1-TAP*::*TRP1 BUD20-3HA*::*HIS3 ura3-52 his3Δ200 trp1Δ63 leu2Δ1*	This study
Y5129 Nsa1-TAP Bud20-HA	*MAT*α *Nsa1-TAP*::*TRP1 BUD20-3HA*::*HIS3 ura3-52 his3Δ200 trp1Δ63 leu2Δ1*	This study
Y3298 Rix1-TAP Bud20-HA	*MAT*α *RIX1-TAP*::*TRP1 BUD20-3HA*::*HIS3 ura3-52 his3Δ200 trp1Δ63 leu2Δ1*	This study
Y3300 Arx1-TAP Bud20-HA	*MAT*α *ARX1-TAP*::*TRP1 BUD20-3HA*::*HIS3 ura3-52 his3Δ200 trp1Δ63 leu2Δ1*	This study
Y3301 Lsg1-TAP Bud20-HA	*MAT*α *LSG1-TAP*::*TRP1 BUD20-3HA*::*HIS3 ura3-52 his3Δ200 trp1Δ63 leu2Δ1*	This study
Y2151 Arx1-TAP	*MAT*α *ura3-52 his3Δ200 trp1Δ63 leu2Δ1 ARX1-TAP*::*TRP1*	40
Arx1-TAP bud20Δ	*MAT*α *ura3-52 his3Δ200 trp1Δ63 leu2Δ1 ARX1-TAP*::*TRP1 bud20*::*HIS3MX*	This study
Bud20 YFP	*MAT*α *leu2 ura3 his3 trp1 BUD20-YFP*::*spHIS5*	This study
Bud20 YFP yvh1Δ	*MAT*α *leu2 ura3 his3 trp1 BUD20-YFP*::*spHIS5 yvh1*::*KanMx6*	This study
Bud20 YFP rei1Δ	*MAT*α *leu2 ura3 his3 trp1 BUD20-YFP*::*spHIS5 rei1*::*natNT2*	This study
HHY110 derivatives	*MAT*α *leu2 ura3 his3 ade2 tor1-1 fpr1*::NAT *PMA1-2xFKBP12*::*TRP1*	16
HHYNog1	See HHY110; *NOG1-FRB-GFP*::*KanMx6*	This study
HHYArx1	See HHY110; *ARX1-FRB-GFP*::*KanMx6*	This study
HHYNop7	See HHY110; *NOP7-FRB-GFP*::*KanMx6*	This study
HHYMrt4	See HHY110; *MRT4-FRB-GFP*::*KanMx6*	This study
HHYRix1	See HHY110; *RIX1-FRB-GFP*::*KanMx6*	This study
HHYBud20	See HHY110; *BUD20-FRB-GFP*::*KanMx6*	This study
HHYNop53	See HHY110; *NOP53-FRB-GFP*::*KanMx6*	This study
HHYTif6	See HHY110; *TIF6-FRB-GFP*::*KanMx6*	This study
HHYAlb1	See HHY110; *ALB1-FRB-GFP*::*KanMx6*	This study
HHYErb1	See HHY110; *ERB1-FRB-GFP*::*KanMx6*	This study
HHYEcm1	See HHY110; *ECM1-FRB-GFP*::*KanMx6*	This study
Arx1-TAP derivatives	*MAT*α *leu2 ura3 his3 trp1 ARX1-TAP*::*TRP1*	42
Arx1-TAP Bud20-YFP	See Arx1-TAP; *BUD20-YFP*::*spHIS5*	This study
Arx1-TAP drg1-ts	*MAT*α *leu2 ura3 his3 trp1 drg1-18 ARX1-TAP*::*TRP1*	42
Arx1-TAP drg1-ts Bud20-YFP	See Arx1-TAP drg1-ts; *BUD20-YFP*::*spHIS5*	This study
Alb1-TAP	*MAT***a** *leu2 ura3 his3 met15 ALB1-TAP*::*HIS3*	This study
Bud20-TAP derivatives	*MAT*α *leu2 ura3 his3 trp1 BUD20-TAP*::*HIS3*	This study
Bud20-TAP drg1-ts	*MAT*α *leu2 ura3 his3 trp1 drg1-18 BUD20-TAP*::*HIS3*	This study
W303	*MAT***a** *ade2 ura3 his3 leu2 trp1*	S. D. Kohlwein
FWY111	*MAT***a** *ura3 leu2 his3 ade2 trp1 afg2-18*	61
Arx1-YFP	See W303; *ARX1-YFP*::*spHIS5*	This study
Arx1-YFP_drg1-18	See FWY111; *ARX1-YFP*::*spHIS5*	This study
Bud20-YFP	See Arx1-TAP strain; *BUD20-YFP*::*spHIS5*	This study
Bud20-YFP_drg1-18	See Arx1-TAP_drg1-18 strain; *BUD20-YFP*::*spHIS5*	This study
Nog1-GFP	*MAT*α *leu2 ura3 his3 met15 NOG1-GFP*::*HISMX6*	42
Nog1-GFP_drg1-18	*MAT***a** *leu2 ura3 his3 trp1 met15 afg2-18 NOG1-GFP*::*HISMX6*	42
Tif6-GFP	*MAT*α *leu2 his3 ade2 trp1 ura3 TIF6-GFP*::*HISMX6*	42
Tif6-GFP_drg1-18	See FWY111; *TIF6-GFP*::*HISMX6*	42
Nop7-YFP	See W303; *NOP7-YFP*::*spHIS5*	This study
Nop7-YFP_drg1-18	See FWY111; *NOP7-YFP*::*spHIS5*	This study
BY4742 derivates	*MAT***a** *leu2 ura3 his3 lys2*	Euroscarf
BY4742 arx1Δ	*MAT***a** *leu2 ura3 his3 lys2 arx1*::*KanMX4*	This study
BY4742 bud20Δ	*MAT***a** *leu2 ura3 his3 lys2 bud20*::*KanMX4*	This study
BY4742 arxΔ bud20Δ	*MAT***a** *leu2 ura3 his3 lys2 arx1*::*KanMX4 bud20*::*natNT2*	This study
PSY967 Kap123Δ	*MAT*α *ura3-52 leu2Δ1 his3Δ200 kap123*::*HIS3*	48
Y2456 Nmd3 shuffle	*MAT*α *trp1 his3 leu2 ura3 nmd3*::*KanMX* pRS316 *NMD3*	11

shows the calculated model (25) of yeast Bud20 based on the NMR structure of human Bud20 (17) (Protein Data Bank [PDB] accession number 1ZR9). The central zinc ion is coordinated by two conserved cysteine and histidine residues. Although the exact function of human Bud20 (ZNF593) is unknown, it was identified previously as a negative modulator of transcription factor Oct-2 in mammalian cells (53). Consistent with an important function of the protein, the deletion of *BUD20* in *S. cerevisiae* results in a slow-growth phenotype in a temperature range from 23°C to 37°C (Fig. 1D). The expression

TABLE 2 Plasmids used in this study

Plasmid	Relevant information	Reference or source
pBUD20	pRS315 *BUD20 LEU2*	This study
pRS314 Bud20	*TRP1*	This study
pRS315 Bud20	*LEU2*	This study
pRS315 Bud20-TAP	*LEU2*	This study
pRS315 Bud20-eGFP	*LEU2*	This study
pRS315 Bud20 ΔNLS eGFP	Deletion of K7 to R16	This study
pRS315 Bud20-NLS* eGFP	K12G R13G R14G	This study
pRS315 Bud20 ΔNESL eGFP	Deletion of L18 to V31	This study
pRS315 Bud20 NES* eGFP	L18R I21R L25R	This study
pRS315 Bud20 N eGFP	Bud20 M1 to P38	This study
pRS315 Bud20 N-NESL* eGFP	Bud20 M1 to P38; L18R I21R L25R	This study
pRS315 Bud20 N-NLS* eGFP	Bud20 M1 to P38; K12G R13G R14G	This study
pRS315 Bud20 CCAA TAP	Bud20 C51A, C54A, TAP	This study
Rpl25-GFP	pRS316 *RPLl25-GFP*	11
Rps2-GFP	pRS316 *RPS2-GFP*	36
pFA6a-FRB-GFP-KanMX6	Cassette for C-terminal FRB-GFP tagging	16
pFA6a-natNT2	Cassette for disruption	
pRS313 NMD3	*HIS3*	11
pRS313 nmd3-2	*HIS3*	11
pRS313 nmd3ΔNES1-GFP	*HIS3*	11
pRS314 MEX67	*TRP1*	49
pRS314 mex67-5	*TRP1*	49
pRS314 mex67KRAA	*TRP1*	59
pRS315 MTR2	*LEU2*	46
pRS315 mtr2-33	*LEU2*	1
pRS315 mtr2-21	*LEU2*	46
pRS314 ECM1	*TRP1*	1
pRS315 ARX1	*LEU2*	6
pRS314 DBP10	*TRP1*	2
pRS314 dbp10-2	*TRP1*	2
pRS314 zz NOC3	*TRP1*	This study
pRS314 zz noc3-1	*TRP1*	35
YCpGAL-YRB4	P_{Gal}-Yrb4 (=Kap123) CEN URA3	47
NESTP	pRS315 nmd3ΔNES1 + 2-eGFP	This study
NESTP-NMD3 NES	pRS315 nmd3ΔNES1 + 2-eGFP-NMD3 NES1	This study
NESTP-PKI NES	pRS315 nmd3ΔNES1 + 2-eGFP-PKI NES1	This study
NESTP-REV NES	pRS315 nmd3ΔNES1 + 2-eGFP-REV NES1	This study
NESTP-BUD20 NES	pRS315 nmd3ΔNES1 + 2-eGFP-Bud20NES (15–39 amino acids)	This study
pHFBud20WT	pYFP-FRB-BUD20	This study
pHFBud20ΔNESL	pYFP-FRB-bud20ΔNESL deletion of L18 to V31	This study
pHFBud20ΔNES	pYFP-FRB-bud20ΔNLS deletion of K7 to R16	This study

of human Bud20 was able to complement the *bud20*Δ slow-growth phenotype (Fig. 1D) despite having a shorter C terminus than the yeast protein (Fig. 1B). This result demonstrates that the function of Bud20 is conserved from yeast to human.

In order to confirm a role for Bud20 in ribosome biogenesis, we tested whether Bud20 associates with ribosomal subunits. Therefore, we fused Bud20 at its C terminus with the TAP tag in order to analyze its sedimentation behavior in sucrose gradients. Bud20-TAP, which fully complemented a *bud20*Δ strain (data not shown), was detected both in the soluble fractions and in fractions containing 60S ribosomal particles (Fig. 2A). In contrast, Bud20-TAP was not associated with polysomes, which also contain mature 60S subunits involved in translation. These data suggest that Bud20 is associated with pre-60S particles, which is consistent with previously reported observations that Bud20 copurifies with preribosomal particles (12, 13, 22). As several ribosomal proteins interact with rRNA through zinc fingers (4, 43), we speculated that Bud20 is targeted to pre-60S particles through its conserved zinc finger domain. To prove this assumption, we created a Bud20 mutant that is defective in zinc binding by the mutation of the two conserved cysteine residues to alanine (C51A and C54A [CCAA]). This *bud20* CCAA mutant was not able to complement the slow-growth phenotype of the *bud20*Δ strain (data not shown) and displayed a significant decrease in the number of 60S subunit particles in the ribosome profile (Fig. 2A). Moreover, this sucrose gradient analysis revealed that the *bud20* CCAA mutant failed to cosediment with ribosomal particles, confirming our assumption that Bud20 binds to pre-60S particles via its zinc finger domain.

In order to determine the 60S intermediates that contain Bud20, we purified pre-60S particles from different maturation stages and analyzed them for the presence of Bud20. Therefore, we fused Bud20 with a triple-hemagglutinin (3HA) tag and TAP purified different pre-60S particles, including early nucleolar (Ssf1 and Nsa1), nuclear (Rix1 and Arx1), and late cytoplasmic (Lsg1) 60S intermediates (30, 40) (Fig. 2B). Western blot analysis revealed that Bud20 was absent in early nucleolar (Ssf1) and late

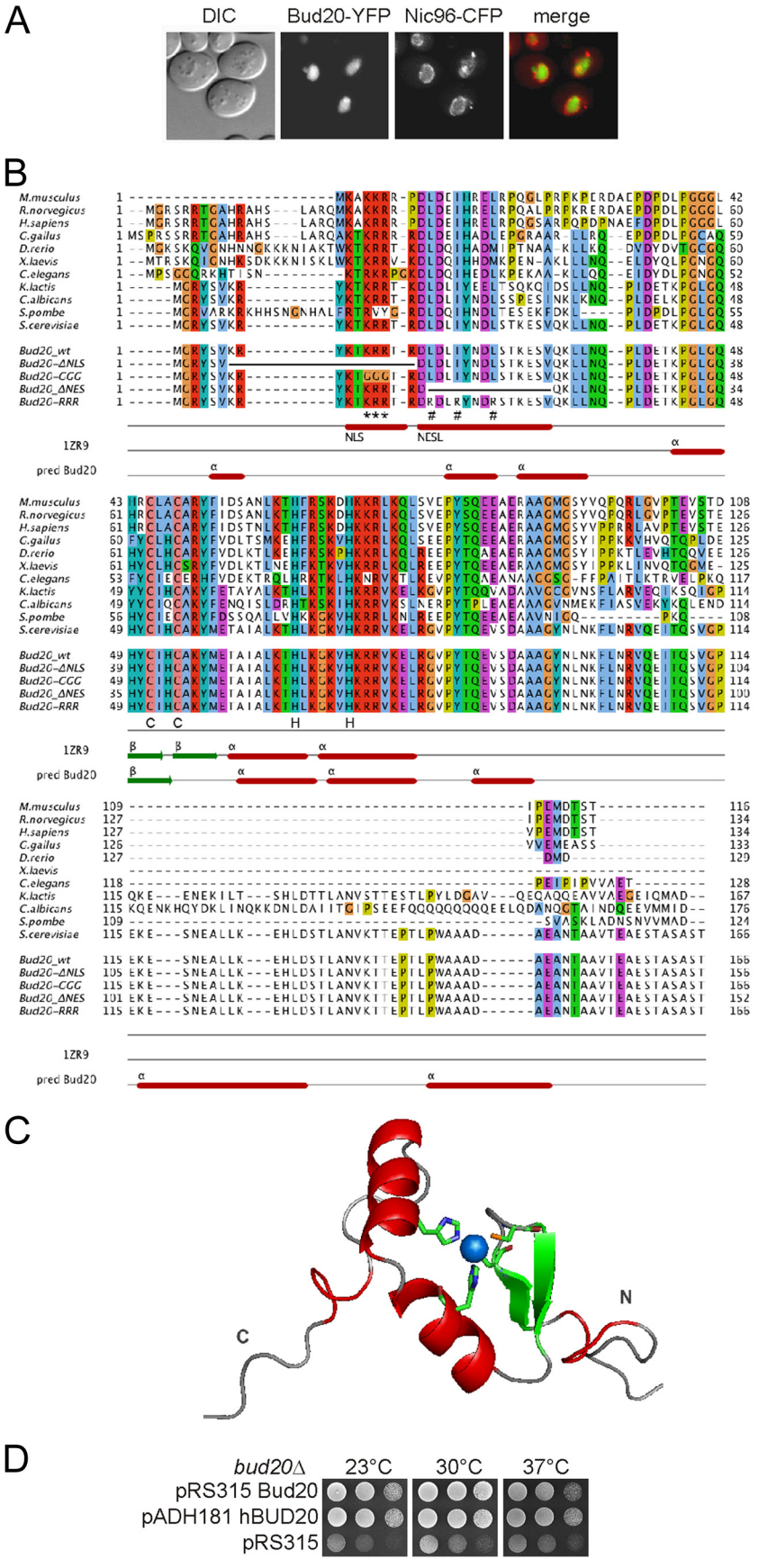
A
DIC
Bud20-YFP
Nic96-CFP
merge
B
M.musculus
R.norvegicus
H.sapiens
C.gallus
D.rerio
X.laevis
C.elegans
K.lactis
C.albicans
S.pombe
S.cerevisiae
Bud20_wt
Bud20-ΔNLS
Bud20-CGG
Bud20_ΔNES
Bud20-RRR
NLS
NESL
1ZR9
pred Bud20
C
N
C
D
bud20Δ
23°C
30°C
37°C
pRS315 Bud20
pADH181 hBUD20
pRS315

cytoplasmic (Lsg1) particles but was significantly enriched in the nucleoplasmic Rix1 particle and in particles purified with the shuttling protein Arx1 (Fig. 2B). These results indicate that Bud20 joins the particle at a late nucleolar or early nucleoplasmic stage of maturation and is released from the Arx1 particle either in the nucleoplasm or in the cytoplasm.

To determine the binding partners of Bud20, we analyzed the protein composition of the preribosomal particles that copurified with Bud20-TAP and compared it to that of the particles purified with Arx1-TAP and Alb1-TAP. As shown in Fig. 2C, Bud20 copurified larger amounts of the nuclear factors Sda1, Nog1, Nop7, Nug1, Rsa4, Rlp7, and Nog2 than either Alb1 or Arx1. This result is consistent with Bud20 binding earlier to the pre-60S particle than Alb1 and Arx1 (6, 10, 40) (Fig. 2B). Since Nog1 was present in prominent amounts in the Bud20 purification, it is likely that it is associated with the Bud20 pre-60S particle throughout its lifetime. As Nog1 and Bud20 are present in the Arx1 particle but are absent from the late cytoplasmic Lsg1 particle (Fig. 2B), both proteins may leave the pre-60S particles at approximately the same time. Another obvious difference is that, in contrast to the Alb1 and Arx1 particles, Rpp0 was not present in the Bud20 particle, while it contained larger amounts of Mrt4 than the Alb1 and Arx1 particles. Since Rpp0 and Mrt4 share the same binding site on the preribosome and Mrt4 is exchanged for Rpp0 in the cytoplasm (26, 33), Bud20 appears to leave the particle before this exchange takes place. This hypothesis is supported by the observation that the strictly cytoplasmic protein Rei1 (31) was completely missing from the Bud20 particle, demonstrating that Bud20 leaves before Rei1 joins the particle. Significantly, the cytoplasmic AAA-ATPase Drg1, which joins the pre-60S particle shortly after export but is absent from late cytoplasmic pre-60S particles, was present on the Bud20 particle. This finding suggests that Bud20 accompanies the pre-60S particle into the cytoplasm and is released shortly after export.

Anchor-away technology identifies Bud20 as a shuttling protein. To prove that Bud20 is a shuttling biogenesis factor, we applied the anchor-away technology (16). This technique is based on the formation of a tight complex of human FKBP12 and FRB (FKBP12-rapamycin binding domain) in the presence of rapamycin. Since rapamycin interferes with yeast growth, these analyses were performed with the rapamycin-resistant *tor1-1* strain. To analyze yeast nuclear export, human FKBP12 is fused to the abundant plasma membrane ATPase Pma1 (16). Therefore, FRB-tagged nuclear proteins that shuttle to the cytoplasm will be trapped at the plasma membrane in the presence of rapamycin. As predicted, the known shuttling factor Arx1, fused to FRB-GFP, relocalized from the nucleus to the cytoplasmic membrane within 15 min of rapamycin treatment. In contrast, the localization of an FRB-GFP fusion of the strictly nuclear factor Nop7 was unaffected even after 90 min of treatment with rapamycin (Fig. 3A). The relocalization of Nop7-FRB-GFP to the cytoplasmic membrane occurred only after a very long treatment with rapamycin (i.e., 16 h), which is most likely due to the trapping of newly synthesized Nop7 in the cytoplasm, restraining its import into the nucleus. The significant difference in the time spans from rapamycin application until accumulation at the plasma membrane makes the anchor-away technology a powerful method to discriminate between shuttling and nonshuttling proteins in ribosome biogenesis.

Next, we tagged Bud20 and known shuttling (i.e., Nog1, Tif6, Arx1, Alb1, Mrt4, and Ecm1) and nonshuttling (Nop53, Rix1, and Erb1) proteins involved in pre-60S maturation with FRB-GFP. These genes were fully functional with a C-terminal FRB-GFP tag. In the presence of rapamycin, the growth of the strains expressing FRB-GFP-tagged versions of the essential proteins Nog1, Tif6, Erb1, Nop53, Nop7, and Rix1 was completely prevented (Fig. 3D). In contrast, the growth of strains expressing the nonessential factors Arx1, Alb1, and Ecm1 fused with FRB-GFP remained unaffected by the drug. The strains with the Mrt4- and Bud20-tagged genes showed slow-growth phenotypes only in the presence of rapamycin (Fig. 3D). Consistent with this result, the deletion of *MRT4* and *BUD20* resulted in a slow-growth phenotype (26, 33) (Fig. 1D). The strict correlation between growth defects caused either by depletion or by rapamycin treatment of the respective FRB fusion strain provides an important control for proving the functionality of the FRB fusion protein (16).

The strains with the FRB-tagged pre-60S maturation factors were inspected by fluorescence microscopy after treatment with rapamycin for various times. As shown in Fig. 3B, Bud20 as well as known shuttling proteins (Nog1, Tif6, Arx1, Alb1, Mrt4, and Ecm1) accumulated at the cytoplasmic membrane after rapamycin treatment and thus could be confirmed as shuttling factors. In contrast, the localization of Nop53, Nop7, Rix1, and Erb1 was not affected by rapamycin treatment for 1 h (Fig. 3C), consistent with a nuclear release of the factors (3, 54). Interestingly, Bud20, Arx1, Mrt4, Ecm1, and Alb1 were completely trapped at the cytoplasmic membrane after 30 min of rapamycin treatment, while Nog1 and Tif6 showed residual nuclear levels after this time period. This finding could be explained by a longer nucle(ol)ar residence time of Nog1 and Tif6, as both proteins bind to the pre-60S particle at an early stage of maturation. In order to exclude any effects from the newly synthesized protein, we incubated the cells with the

FIG 1 Bud20 is a nuclear zinc finger protein associated with pre-60S particles. (A) Fluorescence microscopy of Bud20-YFP. Bud20 was tagged with YFP in a strain expressing a plasmid-borne fusion of cyan fluorescent protein (CFP) with the nuclear pore protein Nic96, and the localization of both proteins was monitored by fluorescence microscopy. The right panel shows an overlay of the signal for nucleus-localized Bud20-YFP and the nuclear pore-associated Nic96-CFP. DIC, differential interference contrast. (B) Multiple-sequence alignment of Bud20 with its orthologs from various eukaryotic organisms (including *Mus musculus*, *Rattus norvegicus*, *Homo sapiens*, *Gallus gallus*, *Danio rerio*, *Xenopus laevis*, *Caenorhabditis elegans*, *Kluyveromyces lactis*, and *Candida albicans*). The alignment was generated with ClustalW (37) and displayed with Jalview (56). Below the alignment, the positions of the generated mutations in the NLS and the NES-like sequence are indicated with asterisks and number signs, respectively. Structural elements (α-helices and β-strands) according to secondary structure predictions (jnetpred) and the structure of human Bud20 (ZNF593) (PDB accession number 1ZR9) (17) are shown. Homology indicates that the zinc ion is coordinated by the conserved residues Cys51, Cys54, His67, and His73, which are indicated below the sequence alignment. (C) The structure model of *S. cerevisiae* Bud20 was calculated by one-to-one treading based on the NMR structure of the human ortholog ZNF593 (PDB accession number 1ZR9) (17) using Phyre2 (25) and displayed using Pymol. The zinc ion, shown as a blue sphere, is coordinated by Cys51, Cys54, His67, and His73, depicted as sticks. (D) Growth analysis of the Bud20 deletion strain. The deletion of *BUD20* results in a pronounced slow-growth phenotype at all tested temperatures, which can be complemented by human ZNF593. The *bud20*Δ *S. cerevisiae* strain was transformed with centromeric plasmid pRS315 harboring *BUD20* or the human ortholog ZNF593/hBud20. Cells were spotted in 10^{-1} serial dilution steps onto SDC plates lacking Leu and incubated at the indicated temperatures for 2 days.

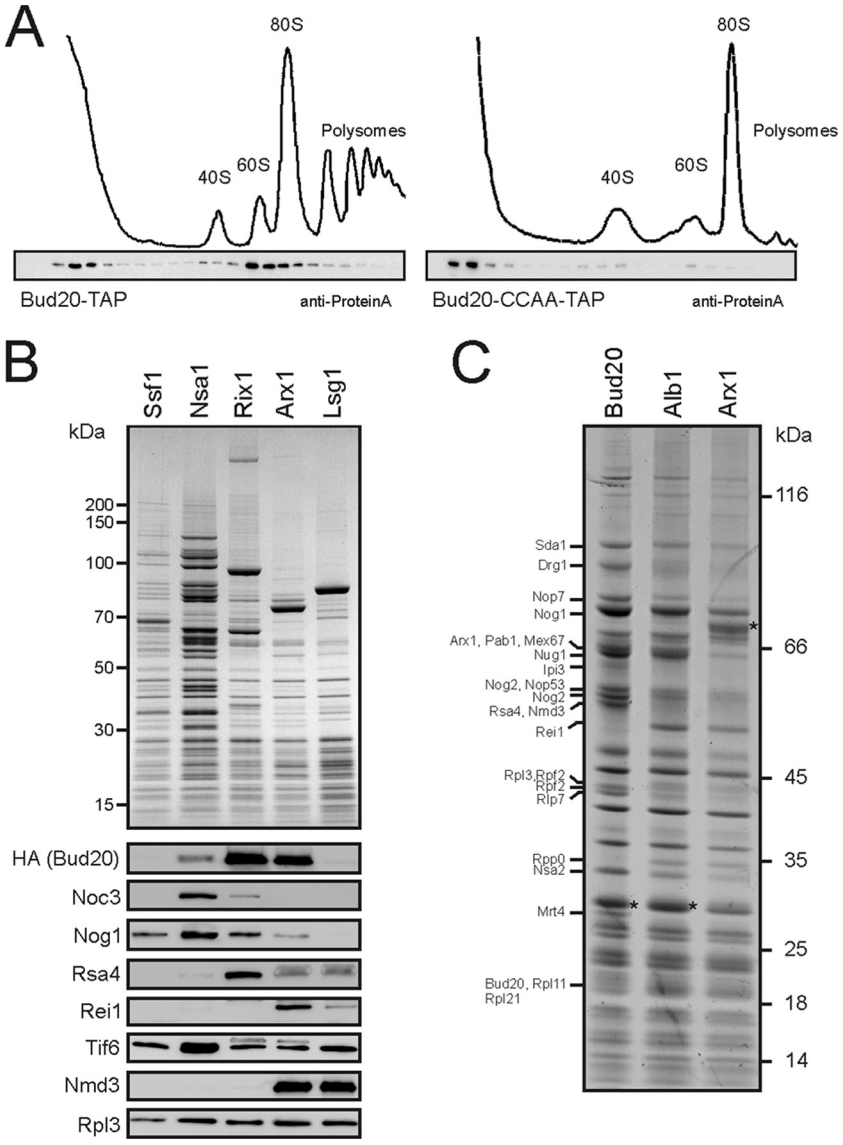

FIG 2 Bud20 is associated with late nuclear and early cytoplasmic pre-60S particles. (A) Sucrose gradient analysis of Bud20-TAP and Bud20 CCAA-TAP. The UV profile recorded at 254 nm is shown at the top. The bottom panel shows Western blots of the fractionated gradient using an anti-protein A antibody. (B) Pre-60S particles from early to late intermediates were TAP purified with the indicated bait proteins from a Bud20-HA strain background. Calmodulin eluates were analyzed by 4 to 12% gradient SDS-PAGE and Coomassie staining (top) or Western blot analysis (bottom). Note that the background in the Tif6 blot is caused by the HA antibody detecting Bud20-HA and that the background in the Rsa4 blot is caused by previous Nmd3 detection. (C) Comparative proteomics of pre-60S particles purified with TAP-tagged Bud20, Alb1, or Arx1 bait proteins. Calmodulin eluates were analyzed by SDS-PAGE and Coomassie staining. Protein bands enriched in the individual preparations were identified by electrospray ionization (ESI) mass spectroscopy and are indicated on the left. The asterisks denote the respective bait proteins.

translational inhibitor cycloheximide and rapamycin in parallel. However, no influence of cycloheximide was observed (data not shown). Taken together, our results showed that Bud20 is a late 60S subunit biogenesis factor, which shuttles between the nuclear and cytoplasmic compartments.

Bud20 is released from the pre-60S particle very early in the cytoplasm. Next, we aimed to determine at which stage Bud20 is released from cytoplasmic pre-60S particles. Previously, it was shown that the AAA-ATPase Drg1 initiates the cytoplasmic maturation of pre-60S particles (32, 42). The inactivation of Drg1 results in a failure to release shuttling pre-60S maturation factors (Nog1 and Rlp24) from preribosomal particles and causes their accumulation in the cytoplasm (42). To test whether the cytoplasmic dissociation of Bud20 requires functional Drg1, we investigated the localization of Bud20-YFP in the temperature-sensitive *drg1-18* mutant. In the wild-type strain, Bud20-YFP showed a predominantly nucleoplasmic steady-state localization at both temperatures, whereas Bud20 accumulated in the cytoplasm upon a 1-h shift of the *drg1-18* mutant to 37°C (Fig. 4A). Purifications of late pre-60S particles via Arx1-TAP from the *drg1-ts* mutant contained increased levels of Bud20-YFP, confirming that the protein remained bound to the preribosome (Fig. 5A).

To characterize this pre-60S particle in more detail, we purified Bud20-TAP from the *drg1-ts* strain. Similarly to Bud20-YFP,

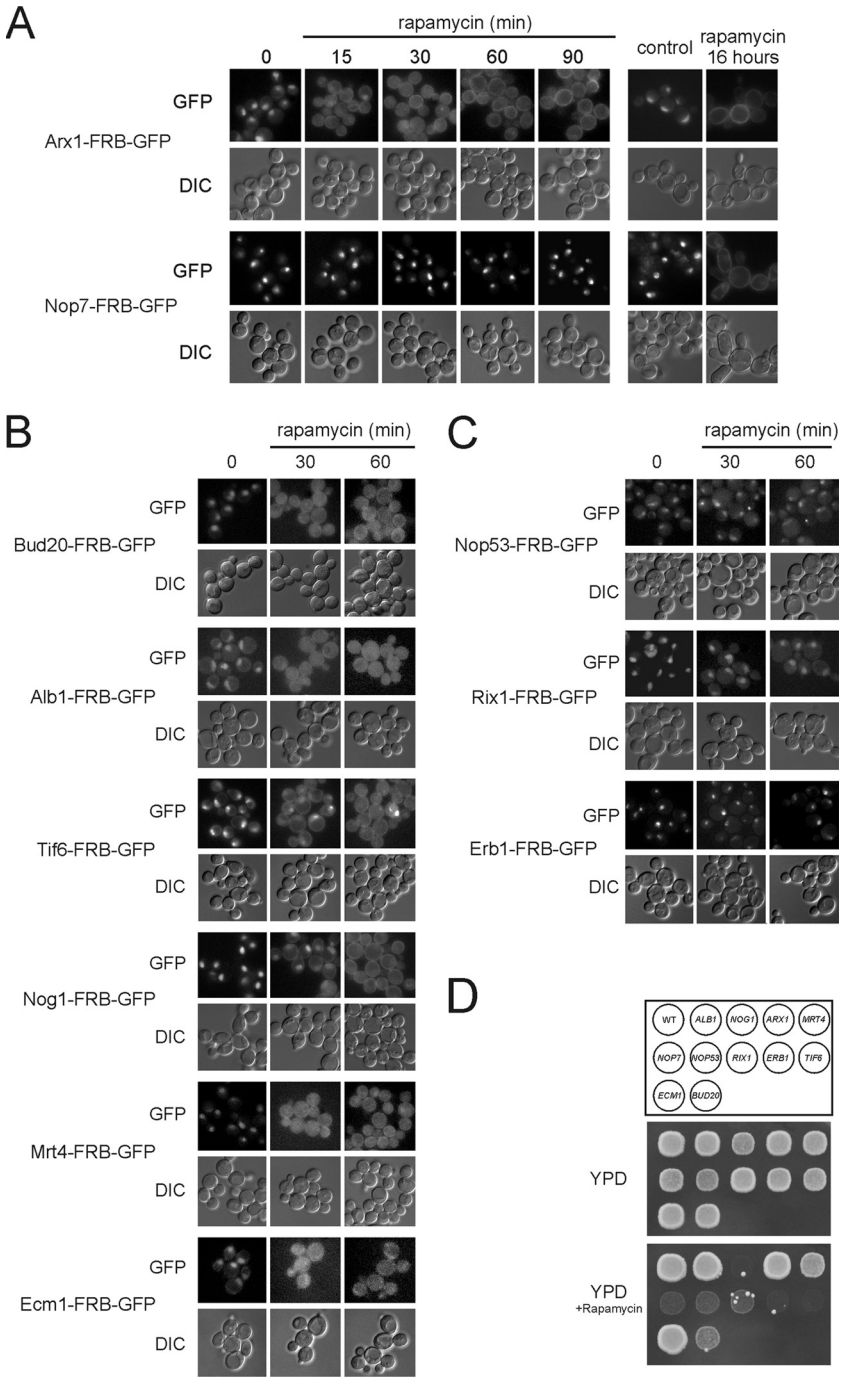

FIG 3 The anchor-away technique revealed shuttling behavior for various 60S biogenesis factors. (A) The anchor-away technique allows discrimination between shuttling proteins such as Arx1 and nuclear factors such as Nop7. Pma1 anchor strain HHY110 (Pma1-FKBP12) was used for the genomic tagging of Arx1 or Nop7 with FRB-GFP. The resulting strains were treated with rapamycin and inspected by fluorescence microscopy after the indicated periods of time. (B) The anchor-away technique demonstrates that Bud20 is a shuttling pre-60S maturation factor. HHY110 strains expressing FRB-GFP fusions of the known shuttling pre-60S maturation factor Alb1, Tif6, Nog1, Mrt4, Ecm1, or Bud20 were treated with rapamycin for 30 or 60 min and monitored by fluorescence microscopy. (C) Fusion proteins of Nop53, Rix1, and Erb1 served as negative controls. (D) Growth analysis of FRB-GFP-tagged 60S biogenesis factors. Pma1 anchor strain HHY110 was used for the genomic tagging of different pre-60S maturation factors with FRB-GFP. The growth phenotype of the resulting strains was analyzed by spotting them onto YPD plates or YPD plates containing 1 μg/ml rapamycin and incubating the plates at 30°C for 3 days. The top panel indicates the positions of the different strains.

Bud20-TAP also accumulated in the cytoplasm upon Drg1 inactivation (data not shown). The TAP purification of Bud20 from the *drg1-ts* strain yielded a pre-60S particle with decreased levels of nuclear factors, including Sda1, Nop7, Nsa2, Rsa4, Rpf2, and Rlp7 (Fig. 5B and C, compare lanes 2 and 4). Moreover, Drg1 was absent from the Bud20 particle in the mutant background, consistent with our previously reported finding that the Drg1-18 protein fails to bind to pre-60S particles (42) (Fig. 5B). In addition,

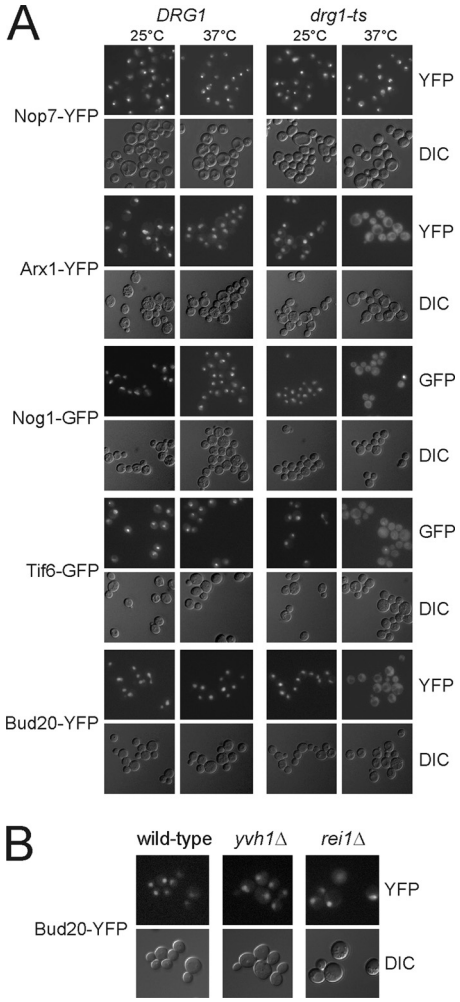

FIG 4 Bud20 accumulates in the cytoplasm of the *drg1-ts* mutant at a restrictive temperature. (A) Bud20 was tagged with YFP in the *DRG1* strain or the temperature-sensitive *drg1-ts* strain. The respective strains were incubated for 1 h at the restrictive temperature of 37°C and inspected by fluorescence microscopy. Wild-type and mutant strains expressing fluorescent versions of the nuclear-resident protein Nop7 or the known shuttling protein Arx1, Nog1, or Tif6 served as controls. (B) Deletion of Yvh1 or Rei1 has no effect on Bud20-YFP localization. *BUD20* was tagged with YFP in *yvh1* and *rei1* deletion strains. Strains were inspected for the localization of Bud20-YFP by fluorescence microscopy.

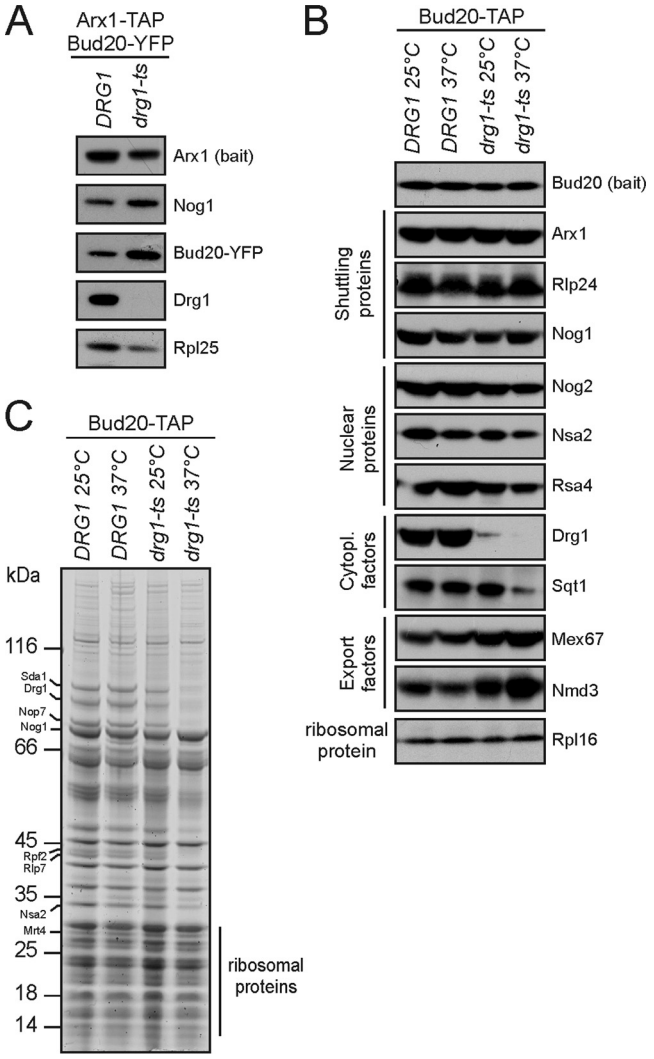

FIG 5 Bud20 accumulates on pre-60S particles from the temperature-sensitive *drg1-ts* mutant. (A) Cytoplasmic Bud20-YFP stays associated with late pre-60S particles in the *drg1-ts* background at a restrictive temperature. *DRG1* wild-type and *drg1-ts* cells coexpressing Arx1-TAP and Bud20-YFP were shifted for 1 h to the restrictive temperature of 37°C before the TAP purification protocol was applied. Pre-60S particles were analyzed by SDS-PAGE and Western blotting using antibodies directed against different biogenesis factors or anti-GFP antibody for Bud20 detection. (B and C) Composition of Bud20-containing preribosomal particles isolated from *DRG1* and *drg1-ts* strains. Strains were grown for 1 h at 37°C before cells were harvested and lysed. Bud20 was TAP purified, and the final calmodulin eluate was analyzed by SDS-PAGE and Coomassie staining (C) or Western blotting (B). Bud20 was detected by an anti-CBP antibody.

the level of Sqt1 decreased (Fig. 5B), confirming our previously reported observation that the downstream maturation of the preribosome is blocked in the *drg1-ts* background (42; H. Bergler, unpublished results). In contrast, the shuttling proteins Nog1, Rlp24, Mrt4, and Arx1 were present at similar levels in the particles from the wild-type and mutant strains (Fig. 5B and C). This result is consistent with the failure to release these proteins from the pre-60S particle in the *drg1-ts* background (42). In contrast, the export factors Mex67 and Nmd3 accumulated on the Bud20 particle from the *drg1-ts* strain, suggesting that under wild-type conditions, they meet Bud20 only for a short period of time on the same particle. The export factor Xpo1 does not routinely copurify with preribosomes in affinity purifications and consequently could not be detected in significant levels in the TAP eluate. In summary, our data demonstrate that Bud20 accompanies the pre-60S particles from the nucleus to the cytoplasm, where it is released shortly after export.

In order to determine whether the release of Bud20 also depends upon factors that act downstream of Drg1, we analyzed the localization of Bud20 in *rei1*Δ and *yvh1*Δ deletion mutants. The zinc finger protein Rei1 is involved in Arx1 release (31), whereas the phosphatase Yvh1 stimulates the exchange of Mrt4 with P0 (26, 33). Both events occur following the Drg1-dependent maturation event (32). As shown in Fig. 4B, the localizations of Bud20-YFP were similar in the wild-type, *yvh1*Δ, and *rei1*Δ strains, showing that neither functional Yvh1 nor Rei1 is required for the

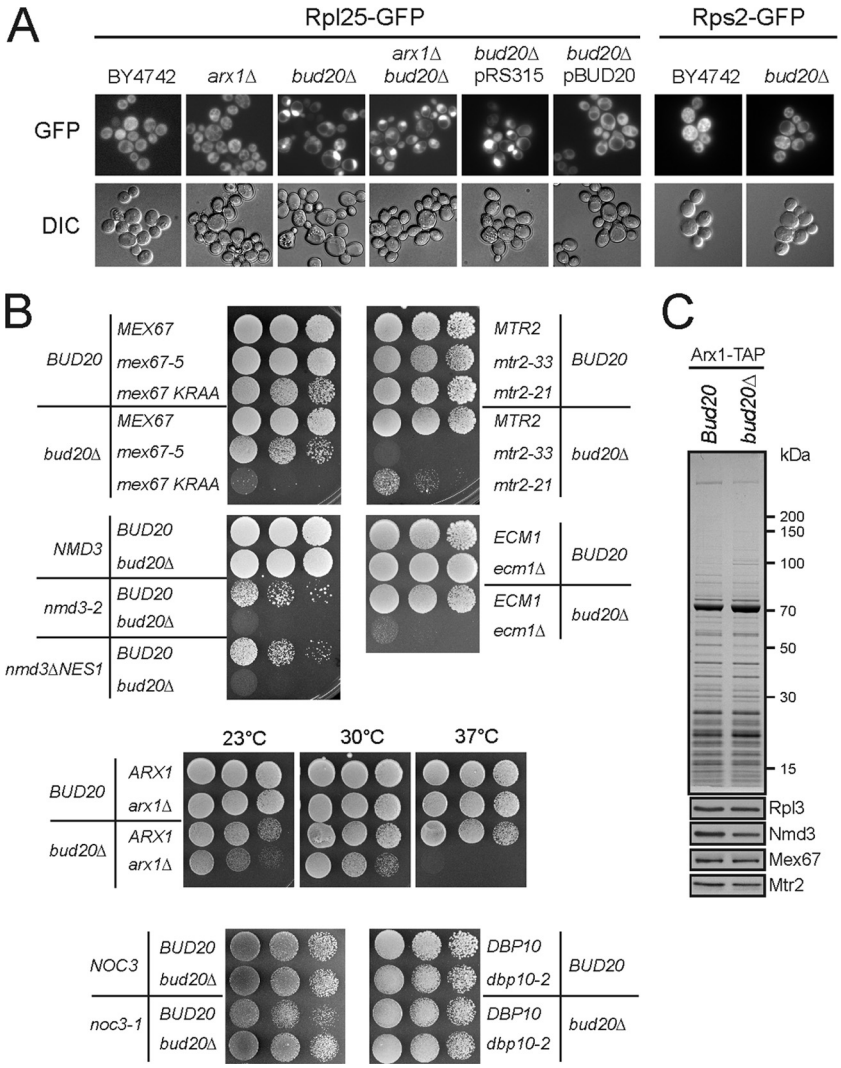

FIG 6 Bud20 is required for pre-60S export. (A) Analysis of preribosome export using large- and small-subunit reporter genes. The Rpl25-GFP reporter (60S subunit) or the Rps2-GFP reporter (40S subunit) was expressed in the indicated strains (derivatives of wild-type strain BY4742) and monitored for nuclear export by fluorescence microscopy. A low-copy-number plasmid (pRS315) carrying the *BUD20* gene under the control of its native promoter (pBUD20) in the *bud20*Δ strain served as a control. (B) *BUD20* exhibits genetic interactions with all tested export factors. Double-deletion strains of different export factors and *bud20* were generated and analyzed for synthetic lethality by transformation with the indicated wild-type and mutant alleles. The *noc3-1* and *dbp10-2* mutants served as controls. The growth phenotype of the transformants was analyzed by spotting 10^{-1} dilution series onto SDC plates with 5-fluoroorotic acid and incubating the plates for 3 to 7 days at 30°C. A lack of growth indicates synthetic lethality. The growth phenotype of the *bud20*Δ *arx1*Δ strain was analyzed on SDC plates lacking Trp and Leu after incubation on SDC plates with 5-fluoroorotic acid. Plates were incubated at the indicated temperatures for 4 days. (C) Deletion of *BUD20* does not significantly alter the association of export factors Arx1, Mex67-Mtr2, and Nmd3 with pre-60S particles. Export-competent pre-60S particles were purified with the Arx1-TAP bait protein from a wild-type background or a *bud20*Δ background. Calmodulin eluates were analyzed by 4 to 12% gradient SDS-PAGE and Coomassie staining and by Western blot analysis using antibodies against the export factors Mex67, Mtr2, and Nmd3. A Western blot with an antibody against the ribosomal protein Rpl3 served as a control.

release of Bud20. Consistently, the prominence of Mrt4 and the lack of Rei1 on the Bud20 particle (Fig. 2C) support the conclusion that Bud20 leaves the pre-60S particle before Yvh1 and Rei1 exert their activities but during or shortly after the time when Drg1 was active.

Bud20 functions in export of the pre-60S particle. Since Bud20 accompanies the pre-60S particles through the nuclear pores, we tested whether Bud20 has a more direct role in pre-60S subunit export. Therefore, we analyzed whether Bud20 is required for the nuclear export of ribosomal subunits and determined the cellular localization of the Rpl25-GFP (large-subunit) and Rps2-GFP (small-subunit) reporters in wild-type and *bud20*Δ cells. Whereas wild-type cells showed a cytoplasmic localization of Rlp25 and Rps2, the deletion of *BUD20* caused a strong nuclear accumulation of Rpl25-GFP but not of Rps2-GFP (Fig. 6A). This result prompted us to test for genetic interactions of the *bud20* null allele with genes involved in pre-60S export. As shown in Fig. 6B, the *bud20*Δ mutant exhibited strong genetic interactions with known pre-60S export factors, including Nmd3, Mex67, Mtr2, Ecm1, and Arx1. Strikingly, synthetic lethality was observed with two different alleles of the export adaptor Nmd3, i.e., *nmd3-2* and *nmd3*Δ*NES1* (11). Furthermore, the *bud20*Δ mutant was syn-

thetic lethal with the 60S export-deficient *mex67*-KRAA allele (59) but not with the *mex67-5* allele, which leads to a specific impairment of mRNA but not ribosome export (46, 49). Additionally, synthetic lethality was observed with the pre-60S export-specific *mtr2-33* allele (1), although retarded growth was also observed in combination with the mRNA-specific *mtr2-21* allele (46). Moreover, the deletion of *BUD20* enhances the cold-sensitive growth phenotype of a strain containing a deletion of the noncanonical export receptor Arx1 (6, 24) and results in synthetic lethality at elevated temperatures. Finally, the combination of *bud20*Δ and *ecm1*Δ mutations was synthetic lethal. In contrast, no synthetic lethality was observed when the *bud20*Δ mutant was combined with the *noc3-1* or *dbp10-2* 60S biogenesis mutant (Fig. 6B). The pronounced genetic interaction of the *bud20*Δ mutant with factors involved in pre-60S export indicates a specific role of Bud20 in 60S subunit export. In order to determine whether Bud20 is required for recruiting known export factors to pre-60S particles, we purified Arx1-TAP from a *bud20*Δ background and determined the association of Mex67-Mtr2 and Nmd3 by Western blot analysis. As shown in Fig. 6C, the deletion of *BUD20* did not influence the recruitment of Arx1, Mex67, Mtr2, or Nmd3 to pre-60S particles. This result shows that Bud20 is not a recruiting factor for other export factors but might play a more direct role in 60S export.

The N-terminal extension of Bud20 harbors motifs resembling an NLS and a NES. *In silico* analyses revealed that in addition to the highly conserved zinc finger motif, Bud20 has a highly conserved N-terminal stretch of about 20 amino acids with a predicted alpha-helical fold. Notably, this conserved N-terminal extension harbors two consecutive motifs, which resemble a classical NLS (nuclear localization signal), followed by a sequence that is partially homologous to the leucine-rich nuclear export signal (NES) (Fig. 7A). Interestingly, the N-terminal half of the NES-like motif, including Φ^0, Φ^1, and Φ^2, displays characteristics of a strong NES, whereas the C-terminal half, carrying Φ^3 and Φ^4, is less homologous and shows variation in the position of Φ^3. To determine whether both motifs are of functional importance *in vivo*, we deleted the putative NLS sequence (ΔNLS) (deletion from K7 to R16) and created point mutations within the NLS-like sequence (NLS*) (K12G, R13G, and R14G mutations) (Fig. 1B). Moreover, we deleted the NES-like sequence (ΔNESL) (D17 to V31) or mutated three of the conserved hydrophobic residues characteristic of the canonical NES (NESL*) (L18R, I21R, and L25R mutations) (Fig. 1B and 7A). The influence of these mutations on the localization of Bud20 was investigated. The localization of the NLS mutants, especially ΔNLS, was shifted slightly toward the cytoplasm (Fig. 7B), whereas the ΔNESL and NESL* mutants were slightly shifted into the nucleus. However, since Bud20 is associated with preribosomes, other signal sequences exposed at the pre-60S particles might contribute to the localization of Bud20. Thus, we aimed to determine the localization behavior of the N-terminal domain containing the putative NLS and NES sequences but lacking the domain for interaction with the preribosome. Therefore, we constructed a Bud20 variant containing the N-terminal domain (amino acid residues 1 to 38) including the putative NLS and NES-like sequences but lacking the zinc finger. Gradient analysis confirmed that the N-terminal domain alone was not able to interact with pre-60S particles (Fig. 7C). Next, we determined the cellular localization of the Bud20 N-terminal domain (Bud20-N). We observed that Bud20-N was local-

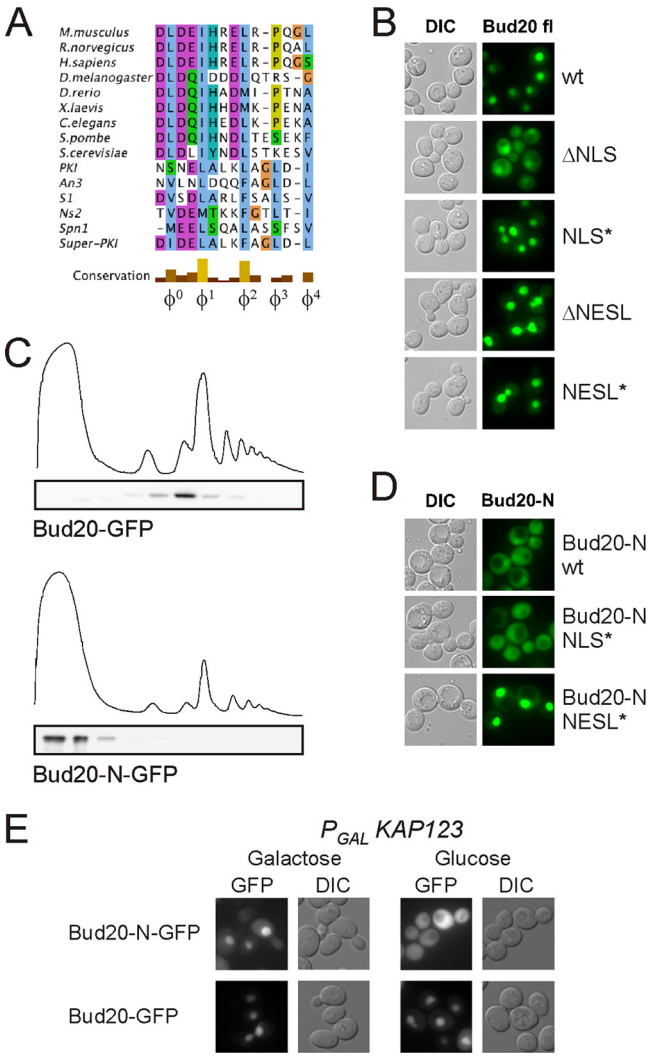

FIG 7 The N-terminal region of Bud20 resembles NES and NLS sequences. (A) Multiple-sequence alignment of the N-terminal region of Bud20 containing the NES-like sequence (NESL) and well-characterized NES sequences (including that of *Drosophila melanogaster*). Below the alignment, the conservation and hydrophobic consensus residues Φ^0, Φ^1, Φ^2, Φ^3, and Φ^4 of canonical NES sequences are indicated. The Bud20 NESL* allele is mutated at positions Φ^0, Φ^1, and Φ^2 (L18R, I21R, and L25R). (B) Localization of the full-length Bud20 protein carrying the indicated mutations or deletions. A wild-type strain, transformed with pRS315 plasmids harboring the indicated Bud20 alleles fused to GFP, was analyzed by fluoresce microscopy. (C) The association of Bud20 and Bud20-N with ribosomal particles was analyzed by sucrose gradient analysis. Lysates of a *bud20*Δ strain, carrying plasmid-borne Bud20-GFP or Bud20-N–GFP, were loaded onto a 10 to 50% sucrose gradient and centrifuged for 16 h at 27,000 rpm. UV profiles recorded at 254 nm are shown above the Western blots of the fractionated gradient with anti-GFP antibody. (D) Mutations in the NLS and NES-like sequence, present in NLS* and NESL*, respectively, affect the cellular localization of the Bud20 N-terminal domain. The constructs were analyzed in the *BUD20* wild-type background. (E) Localization of Bud20-N–GFP and Bud20-GFP in a Kap123-depleted strain. A *kap123*Δ strain (PSY967) was transformed with YCpGAL-Yrb4, encoding Kap123 under the control of a Gal promoter, and with plasmid pRS315-Bud20-GFP or pRS315-Bud20-N-GFP, expressing full-length Bud20 or its N domain fused to GFP, respectively. Cells were grown in galactose (expression of Kap123)- or glucose (repression of Kap123)-containing medium, and the localization of the GFP fusions was inspected by fluorescence microscopy.

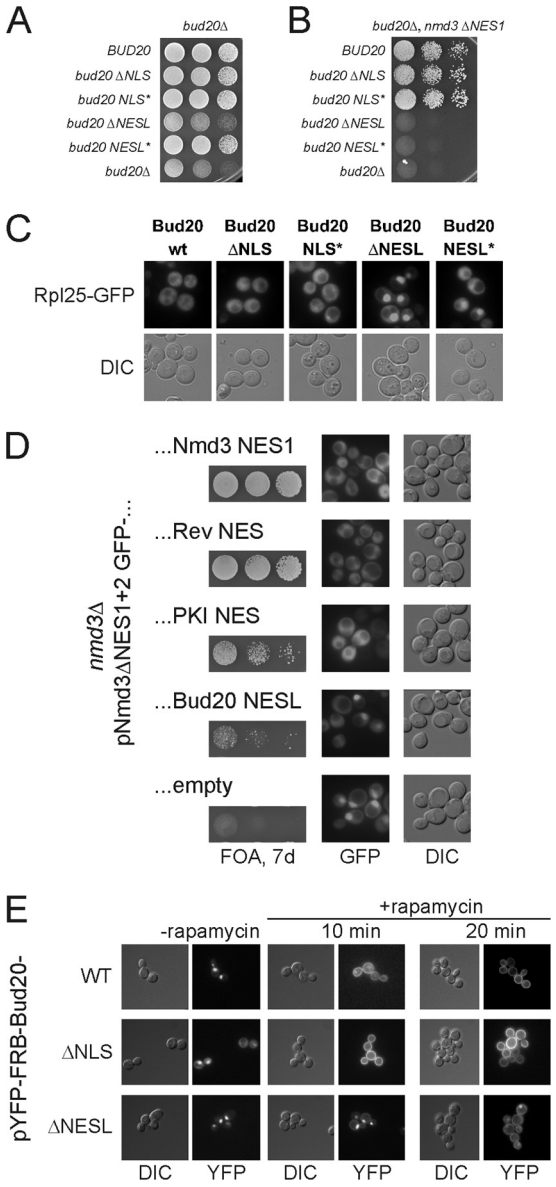

FIG 8 The NES-like sequence of Bud20 is required for pre-60S export and is able to partially replace Nmd3ΔNES. (A) Deletion of the NES-like sequence of Bud20 results in the functional inactivation of the protein. A *bud20*Δ strain was transformed with various pRS315 plasmids expressing the indicated *BUD20* variants and tested for growth on SDC medium lacking Leu. (B) Mutation or deletion of the NES-like sequence of Bud20 is synthetic lethal with mutations in the canonical export adaptor Nmd3. The *bud20*Δ *nmd3*Δ shuffle strain was transformed with plasmids pRS313-nmd3-ΔNES1-GFP and pRS315 coding for the indicated *BUD20* alleles and monitored for growth on SDC plates with 5-fluoroorotic acid. A lack of growth indicates synthetic lethality. (C) Bud20 NESL mutants show an Rpl25 export defect. The *bud20*Δ strain was transformed with the indicated *bud20* allele and the Rpl25-GFP reporter and tested for functional pre-60S export by fluorescence microscopy. (D) The NES-like sequence of Bud20 can partially replace the Nmd3 NES. The *nmd3* shuffle strain was transformed with a pRS315 plasmid with *nmd3ΔNES1+2-GFP* fused with the *BUD20* NES-like sequences (amino acid residues 15 to 34). The analogous plasmids fused with NMD3 NES1, the Rev NES, and the PKI NES or without a NES (empty) served as positive and negative controls, respectively. Growth analysis was done by spotting 10^{-1} serial dilutions onto plates containing 5-fluoroorotic acid (FOA). Pictures were taken after 7 days. Growth on plates containing 5-fluoroorotic acid indicated a complementation of the lethality arising from the deletion of both nuclear export signals of Nmd3. The localization of the corresponding constructs was ized mainly to the nucleoplasm, but a significant pool of the protein was also detected in the cytoplasm (Fig. 7D). The mutation of the NLS or the NES-like sequence in the non-ribosome-associated Bud20 variant resulted in a pronounced mislocalization of the protein. Bud20-N–NLS* was shifted toward the cytoplasm, whereas the mutation of the NES-like sequence (Bud20-N–NESL*) led to a marked nuclear accumulation. These results indicate that the N-terminal extension of Bud20 behaves like NLS and NES motifs.

To find further evidence that Bud20 harbors an NLS in its N-terminal extension, we determined the localization of Bud20-N–GFP in various karyopherin mutants. We observed that the nuclear import of Bud20-N–GFP was inhibited in the *kap123*Δ deletion strain (Fig. 7E), indicating that Bud20 is transported into the nucleus via a Kap123-dependent route (45, 47). However, the NLS sequence was not crucial for the *in vivo* function of Bud20 (Fig. 8A), suggesting that other motifs in Bud20 may contribute to nuclear import. Consistent with that assumption, we observed that full-length Bud20 was able to enter the nucleus in a *KAP123* deletion background (Fig. 7E). Thus, Bud20 is imported via at least two redundant pathways.

Next, we focused on the NES-like sequence (NESL) to find out whether it is crucial for the *in vivo* function of Bud20. Whereas point mutations in this motif largely complemented the *bud20* null mutant, the complete deletion of the NES-like motif generated a slow-growth phenotype comparable to that of the *bud20* null strain (Fig. 8A). Thus, the NES-like motif is strictly required for the *in vivo* function of Bud20. Intriguingly, the point mutations in the NES-like sequence and the complete deletion exhibited synthetic lethality with the *nmd3ΔNES1* allele of the export adaptor Nmd3 (Fig. 8B) and the *mtr2-33* mutant (J. Baßler, unpublished results). These results suggest that the NES-like sequence of Bud20 is strongly coupled to the nuclear export of the pre-60S particle. This is further supported by the finding that both mutants exhibited a pronounced export defect of the Rpl25-eGFP reporter (Fig. 8C). To determine whether the Bud20 NES-like sequence can act as a NES in a heterologous system, we fused the NES-like sequence to a truncated NES variant of the canonical export adaptor Nmd3. This Nmd3ΔNES1+2 variant lacks both NES signals and is therefore nonfunctional in pre-60S export (11, 21). Interestingly, the addition of heterologous NES sequences can suppress the lethal phenotype (20, 21) (Fig. 8D). As shown in Fig. 8D, the addition of the Bud20 NES-like sequence (amino acid residues 15 to 34) to Nmd3ΔNES1+2 can partially restore growth and the cytoplasmic localization. However, the complementation by the Bud20 NES-like sequence was significantly less efficient than the complementation by the bona fide NES sequence of Nmd3, Rev, or PKI (Fig. 8D).

We also analyzed the shuttling behaviors of Bud20 and the Bud20-ΔNESL and Bud20-ΔNLS mutants by using the anchor-

cence microscopy in the presence of a wild-type Nmd3 copy in SDC medium lacking Leu. The cytoplasmic localization or nuclear exclusion of the reporter protein demonstrates the ability to act as an NES sequence. (E) The anchor-away assay confirmed the slower nuclear export of Bud20ΔNESL. Centromeric vectors expressing fusion proteins of YFP with FRB and Bud20 (wild type [WT]) or mutants containing deletions in the NLS (ΔNLS) or the NES-like sequence (ΔNESL) were transformed into Pma1-FKBP12 anchor strain HHY110. The localization of the YFP fusions was monitored by fluorescence microscopy after 10 or 20 min of rapamycin treatment.

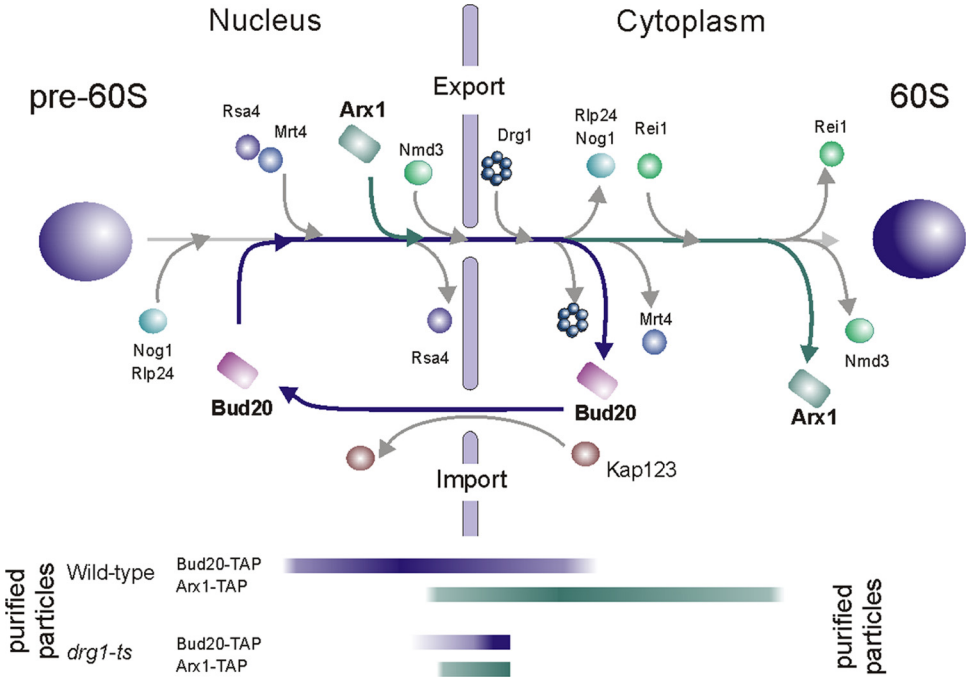

FIG 9 Model of the spatiotemporal order of Bud20 recruitment and release from pre-60S particles. See the text for details.

away technology. As shown in Fig. 8E, the export of YFP–FRB–Bud20-ΔNESL was significantly delayed compared to that of the wild-type protein. This result underlines the role of the NES-like sequence in the nuclear export of Bud20 and is consistent with the accumulation of the Rpl25-GFP reporter in the *bud20ΔNESL* mutant (Fig. 8C).

Taken together, these data demonstrate that Bud20 carries a NES-like sequence motif in its N-terminal extension, which is crucial for the nuclear export of pre-60S subunits.

DISCUSSION

This study has unraveled an unexpected role of the conserved Bud20 in the nuclear export of the pre-60S subunit. Bud20 is imported into the nucleus by the karyopherin Kap123 and associates there with late nuclear pre-60S particles. During the maturation process, it is exported with the pre-60S subunit into the cytoplasm, where it gets released through a mechanism dependent upon the Drg1 AAA-ATPase. However, we do not know whether Bud20 is a direct substrate of Drg1, since a direct functional link between these two proteins has not yet been established. Nevertheless, our cell biological and biochemical data enabled us to define the time point of the association and dissociation of Bud20 with respect to other biogenesis factors (Fig. 9).

No direct binding partner of Bud20 has yet been identified, but we have demonstrated that the association with the preribosome depends on the zinc finger domain of Bud20. Since many zinc finger proteins, including several ribosomal proteins of the small (43) and large (4) subunits, bind directly to nucleic acids, we hypothesize that the zinc finger of Bud20 might bind directly to rRNA. In an attempt to identify this binding site(s) on the rRNA, we utilized the UV cross-linking and cDNA analysis (CRAC) method (14, 15). Unfortunately, because Bud20 inefficiently cross-linked to RNA *in vivo*, we were unable to reliably identify specific Bud20-rRNA interaction sites (S. Granneman, unpublished results). However, this result does not rule out that Bud20 binds directly to rRNA. The identification of RNA binding sites for zinc finger RNA binding proteins with CRAC has generally proven to be quite challenging (S. Granneman, personal communication), indicating that zinc finger-RNA interactions may be difficult to catch by using UV irradiation.

What could be the precise role of Bud20 in ribosome biogenesis? Our findings imply that Bud20 performs an active role in ribosome export, indicated by its exceptionally strong genetic link to other known 60S export factors, including Xpo1-Nmd3, Mex67-Mtr2, and Arx1, which exhibit physical contact with the transport cargo and can dynamically interact with the nuclear pore complex (6, 20, 51, 58). However, recombinant Bud20 does not interact directly with FG-repeat-containing nucleoporins, including Nup1, Nup116, or Nsp1 (H. Bergler and J. Baßler, unpublished data).

Our data demonstrate that a short N-terminal motif that resembles a NES is essential for Bud20 function in pre-60S subunit export. Previously, it was shown that the growth defect of an *nmd3ΔNES1+2* mutant can be rescued by fusing the truncated Nmd3 protein to a NES sequence (20, 21). However, the Bud20 NES-like sequence was not able to fully complement the Nmd3ΔNES1+2 phenotype (Fig. 8D). Furthermore, we did not observe a mislocalization of the Bud20-N–GFP construct in a leptomycin-sensitive *xpo1-T539C* strain, nor did we find recombinant Bud20 to bind to Xpo1 in a RanGTP-dependent mechanism (J. Baßler and E. Thomson, unpublished results). Thus, the NES-like sequence of Bud20 does not show all of the classical NES properties when it is analyzed separated from its native environment on the export-competent preribosome. Still, it could be envisaged that the binding of Bud20 to pre-60S particles induces a conformational change that is necessary for

the formation of a fully functional NES. Alternatively, the NES-like sequence of Bud20 may need to be combined with another signal from a different biogenesis factor on the preribosome, which contributes to stabilize the interaction between Bud20 and Xpo1 to promote ribosomal export. Nevertheless, this NES-like sequence may contribute to the export of ribosomal subunits via another, as-yet-unidentified, mechanism. Therefore, it might be crucial to determine the position of Bud20 at the preribosome and to identify its neighbors to unravel the mechanism of its function in 60S export.

ACKNOWLEDGMENTS

We are indebt to Sander Granneman for performing the CRAC assay. We thank Micheline Fromont-Racine, Bernard L. Trumpower, Juan P. Ballesta, Thomas Gerstberger, Arlen W. Johnson, Miguel Remacha, and Sabine Rospert for generously supplying reagents. We kindly acknowledge the expert help of Jessica Fischer for the binding assay of Bud20 with Nups and of Oliver Domenig for strain construction.

This work was supported by a grant from the Austrian Science Foundation (FWF) (grant P21991) to H.B. and a grant from the Deutsche Forschungsgemeinschaft (grant Hu363/10) to J.B. and E.H.

REFERENCES

1. **Bassler J, et al.** 2001. Identification of a 60S preribosomal particle that is closely linked to nuclear export. Mol. Cell **8**:517–529.
2. **Bassler J, Kallas M, Hurt E.** 2006. The NUG1 GTPase reveals and N-terminal RNA-binding domain that is essential for association with 60 S pre-ribosomal particles. J. Biol. Chem. **281**:24737–24744.
3. **Bassler J, et al.** 2010. The AAA-ATPase Rea1 drives removal of biogenesis factors during multiple stages of 60S ribosome assembly. Mol. Cell **38**: 712–721.
4. **Ben-Shem A, et al.** 2011. The structure of the eukaryotic ribosome at 3.0 A resolution. Science **334**:1524–1529.
5. **Birner-Gruenberger R, Susani-Etzerodt H, Kollroser M, Rechberger GN, Hermetter A.** 2008. Lipolytic and esterolytic activity-based profiling of murine liver. Proteomics **8**:3645–3656.
6. **Bradatsch B, et al.** 2007. Arx1 functions as an unorthodox nuclear export receptor for the 60S preribosomal subunit. Mol. Cell **27**:767–779.
7. **Carr S, et al.** 2004. The need for guidelines in publication of peptide and protein identification data: Working Group on Publication Guidelines for Peptide and Protein Identification Data. Mol. Cell. Proteomics **3**:531–533.
8. **Fatica A, Tollervey D.** 2002. Making ribosomes. Curr. Opin. Cell Biol. **14**:313–318.
9. **Freed EF, Bleichert F, Dutca LM, Baserga SJ.** 2010. When ribosomes go bad: diseases of ribosome biogenesis. Mol. Biosyst. **6**:481–493.
10. **Fromont-Racine M, Senger B, Saveanu C, Fasiolo F.** 2003. Ribosome assembly in eukaryotes. Gene **313**:17–42.
11. **Gadal O, et al.** 2001. Nuclear export of 60S ribosomal subunits depends on Xpo1p and requires a nuclear export sequence-containing factor, Nmd3p, that associates with the large subunit protein Rpl10p. Mol. Cell. Biol. **21**:3405–3415.
12. **Gavin AC, et al.** 2006. Proteome survey reveals modularity of the yeast cell machinery. Nature **440**:631–636.
13. **Gavin AC, et al.** 2002. Functional organization of the yeast proteome by systematic analysis of protein complexes. Nature **415**:141–147.
14. **Granneman S, Kudla G, Petfalski E, Tollervey D.** 2009. Identification of protein binding sites on U3 snoRNA and pre-rRNA by UV cross-linking and high-throughput analysis of cDNAs. Proc. Natl. Acad. Sci. U. S. A. **106**:9613–9618.
15. **Granneman S, Petfalski E, Swiatkowska A, Tollervey D.** 2010. Cracking pre-40S ribosomal subunit structure by systematic analyses of RNA-protein cross-linking. EMBO J. **29**:2026–2036.
16. **Haruki H, Nishikawa J, Laemmli UK.** 2008. The anchor-away technique: rapid, conditional establishment of yeast mutant phenotypes. Mol. Cell **31**:925–932.
17. **Hayes PL, Lytle BL, Volkman BF, Peterson FC.** 2008. The solution structure of ZNF593 from Homo sapiens reveals a zinc finger in a predominantly unstructured protein. Protein Sci. **17**:571–576.
18. **Hedges J, West M, Johnson AW.** 2005. Release of the export adapter, Nmd3p, from the 60S ribosomal subunit requires Rpl10p and the cytoplasmic GTPase Lsg1p. EMBO J. **24**:567–579.
19. **Henras AK, et al.** 2008. The post-transcriptional steps of eukaryotic ribosome biogenesis. Cell. Mol. Life Sci. **65**:2334–2359.
20. **Ho JH, Kallstrom G, Johnson AW.** 2000. Nascent 60S ribosomal subunits enter the free pool bound by Nmd3p. RNA **6**:1625–1634.
21. **Ho JH, Kallstrom G, Johnson AW.** 2000. Nmd3p is a Crm1p-dependent adapter protein for nuclear export of the large ribosomal subunit. J. Cell Biol. **151**:1057–1066.
22. **Ho Y, et al.** 2002. Systematic identification of protein complexes in Saccharomyces cerevisiae by mass spectrometry. Nature **415**:180–183.
23. **Huh WK, et al.** 2003. Global analysis of protein localization in budding yeast. Nature **425**:686–691.
24. **Hung NJ, Lo KY, Patel SS, Helmke K, Johnson AW.** 2008. Arx1 is a nuclear export receptor for the 60S ribosomal subunit in yeast. Mol. Biol. Cell **19**:735–744.
25. **Kelley LA, Sternberg MJ.** 2009. Protein structure prediction on the Web: a case study using the Phyre server. Nat. Protoc. **4**:363–371.
26. **Kemmler S, Occhipinti L, Veisu M, Panse VG.** 2009. Yvh1 is required for a late maturation step in the 60S biogenesis pathway. J. Cell Biol. **186**:863–880.
27. **Kressler D, Hurt E, Bassler J.** 2010. Driving ribosome assembly. Biochim. Biophys. Acta **1803**:673–683.
28. **Kressler D, Hurt E, Bergler H, Bassler J.** 2012. The power of AAA-ATPases on the road of pre-60S ribosome maturation—molecular machines that strip pre-ribosomal particles. Biochim. Biophys. Acta **1823**:92–100.
29. **Kressler D, Linder P, de La Cruz J.** 1999. Protein trans-acting factors involved in ribosome biogenesis in Saccharomyces cerevisiae. Mol. Cell. Biol. **19**:7897–7912.
30. **Kressler D, Roser D, Pertschy B, Hurt E.** 2008. The AAA ATPase Rix7 powers progression of ribosome biogenesis by stripping Nsa1 from pre-60S particles. J. Cell Biol. **181**:935–944.
31. **Lebreton A, et al.** 2006. A functional network involved in the recycling of nucleocytoplasmic pre-60S factors. J. Cell Biol. **173**:349–360.
32. **Lo KY, et al.** 2010. Defining the pathway of cytoplasmic maturation of the 60S ribosomal subunit. Mol. Cell **39**:196–208.
33. **Lo KY, Li Z, Wang F, Marcotte EM, Johnson AW.** 2009. Ribosome stalk assembly requires the dual-specificity phosphatase Yvh1 for the exchange of Mrt4 with P0. J. Cell Biol. **186**:849–862.
34. **Longtine MS, et al.** 1998. Additional modules for versatile and economical PCR-based gene deletion and modification in Saccharomyces cerevisiae. Yeast **14**:953–961.
35. **Milkereit P, et al.** 2001. Maturation and intranuclear transport of pre-ribosomes requires Noc proteins. Cell **105**:499–509.
36. **Milkereit P, et al.** 2003. A Noc complex specifically involved in the formation and nuclear export of ribosomal 40 S subunits. J. Biol. Chem. **278**:4072–4081.
37. **Myers EW, Miller W.** 1988. Optimal alignments in linear space. Comput. Appl. Biosci. **4**:11–17.
38. **Narla A, Ebert BL.** 2010. Ribosomopathies: human disorders of ribosome dysfunction. Blood **115**:3196–3205.
39. **Ni L, Snyder M.** 2001. A genomic study of the bipolar bud site selection pattern in Saccharomyces cerevisiae. Mol. Biol. Cell **12**:2147–2170.
40. **Nissan TA, Bassler J, Petfalski E, Tollervey D, Hurt E.** 2002. 60S pre-ribosome formation viewed from assembly in the nucleolus until export to the cytoplasm. EMBO J. **21**:5539–5547.
41. **Panse VG, Johnson AW.** 2010. Maturation of eukaryotic ribosomes: acquisition of functionality. Trends Biochem. Sci. **35**:260–266.
42. **Pertschy B, et al.** 2007. Cytoplasmic recycling of 60S preribosomal factors depends on the AAA protein Drg1. Mol. Cell. Biol. **27**:6581–6592.
43. **Rabl J, Leibundgut M, Ataide SF, Haag A, Ban N.** 2011. Crystal structure of the eukaryotic 40S ribosomal subunit in complex with initiation factor 1. Science **331**:730–736.
44. **Ribbeck K, Gorlich D.** 2002. The permeability barrier of nuclear pore complexes appears to operate via hydrophobic exclusion. EMBO J. **21**: 2664–2671.
45. **Rout MP, Blobel G, Aitchison JD.** 1997. A distinct nuclear import pathway used by ribosomal proteins. Cell **89**:715–725.
46. **Santos-Rosa H, et al.** 1998. Nuclear mRNA export requires complex formation between Mex67p and Mtr2p at the nuclear pores. Mol. Cell. Biol. **18**:6826–6838.
47. **Schlenstedt G, et al.** 1997. Yrb4p, a yeast ran-GTP-binding protein involved in import of ribosomal protein L25 into the nucleus. EMBO J. **16**:6237–6249.

48. **Seedorf M, Silver PA.** 1997. Importin/karyopherin protein family members required for mRNA export from the nucleus. Proc. Natl. Acad. Sci. U. S. A. **94**:8590–8595.
49. **Segref A, et al.** 1997. Mex67p, a novel factor for nuclear mRNA export, binds to both poly(A)+ RNA and nuclear pores. EMBO J. **16**:3256–3271.
50. **Shevchenko A, Wilm M, Vorm O, Mann M.** 1996. Mass spectrometric sequencing of proteins silver-stained polyacrylamide gels. Anal. Chem. **68**:850–858.
51. **Strasser K, Bassler J, Hurt E.** 2000. Binding of the Mex67p/Mtr2p heterodimer to FXFG, GLFG, and FG repeat nucleoporins is essential for nuclear mRNA export. J. Cell Biol. **150**:695–706.
52. **Strunk BS, Karbstein K.** 2009. Powering through ribosome assembly. RNA **15**:2083–2104.
53. **Terunuma A, Shiba K, Noda T.** 1997. A novel genetic system to isolate a dominant negative effector on DNA-binding activity of Oct-2. Nucleic Acids Res. **25**:1984–1990.
54. **Ulbrich C, et al.** 2009. Mechanochemical removal of ribosome biogenesis factors from nascent 60S ribosomal subunits. Cell **138**:911–922.
55. **Warner JR.** 1999. The economics of ribosome biosynthesis in yeast. Trends Biochem. Sci. **24**:437–440.
56. **Waterhouse AM, Procter JB, Martin DM, Clamp M, Barton GJ.** 2009. Jalview version 2—a multiple sequence alignment editor and analysis workbench. Bioinformatics **25**:1189–1191.
57. **Wente SR, Rout MP.** 2010. The nuclear pore complex and nuclear transport. Cold Spring Harb. Perspect. Biol. doi:10.1101/cshperspect.a000562.
58. **Yao W, Lutzmann M, Hurt E.** 2008. A versatile interaction platform on the Mex67-Mtr2 receptor creates an overlap between mRNA and ribosome export. EMBO J. **27**:6–16.
59. **Yao W, et al.** 2007. Nuclear export of ribosomal 60S subunits by the general mRNA export receptor Mex67-Mtr2. Mol. Cell **26**:51–62.
60. **Yao Y, et al.** 2010. Ecm1 is a new pre-ribosomal factor involved in pre-60S particle export. RNA **16**:1007–1017.
61. **Zakalskiy A, et al.** 2002. Structural and enzymatic properties of the AAA protein Drg1p from Saccharomyces cerevisiae. Decoupling of intracellular function from ATPase activity and hexamerization. J. Biol. Chem. **277**:26788–26795.